ORGANIC CHEMISTRY FRONTIERS

CCS 中国化学会 CHINESE CHEMICAL SOCIETY

SIOC 1950

ROYAL SOCIETY OF CHEMISTRY

RESEARCH ARTICLE

View Article Online
View Journal

Cite this: DOI: 10.1039/d5qo01635e

Densely-functionalized bicyclic cyclopentanones by combined photoinduced 6-*endo-trig* Giese additions and mild aldol cyclizations

Júlia Viñas-Lóbez,†[a] Nicolas Sellet, †[a] Bibiana Fabri, [a] Guillaume Levitre,[a] Adiran de Aguirre,[a] Amalia I. Poblador-Bahamonde, [a] Céline Besnard [b] and Jérôme Lacour *[a]

Polycyclic scaffolds are central to numerous natural products and pharmaceuticals, motivating concise, stereocontrolled routes to their construction. We report a photoredox-enabled synthesis of *trans*-fused [*n*.3.0] bicyclic ketones (*n* = 4, 5, 10) from malonate-derived enol ethers. α-Brominated intermediates, formed by acylation with 2-bromo-2-methylpropanoyl bromide, undergo radical cyclization under two complementary conditions: (i) acridinium orange (**AOH$^+$**) with Hantzsch ester (**HE**) at 455 nm, or (ii) photoexcited **HE** alone at 365 nm. Both modes trigger 6-*endo-trig* Giese addition, C–O bond fragmentation, and hydrogen-atom transfer to α-branched cyclic ketones that ring-close under mild Brønsted or Lewis acid activation to *trans*-fused products with exclusive junction control. Mechanistic studies (Stern–Volmer, UV–Vis, electrochemistry) support two activation pathways—**AOH^{+*}** quenching by **HE** or direct **HE** excitation—each generating the same radical intermediates *in fine*. DFT calculations validate mechanistic pathways and regioselectivity in favor of philicity matching of the electrophilic radical and the polar electron-rich enol ether. The method accommodates ring-size diversity, accesses *trans*-hydrindanone architectures, and outcompetes 5-*exo-trig* spirocyclization.

Received 1st December 2025,
Accepted 26th January 2026

DOI: 10.1039/d5qo01635e

rsc.li/frontiers-organic

Introduction

Polycyclic natural products and medicinal drugs are ubiquitous generating hence a continuous demand for novel cyclization strategies in academic and industrial laboratories alike.[1] Methodologies for ring closures are thus crucial and very diverse approaches are available, from polar bond formations to concerted, organometallic or radical (*vide infra*) pathways.[2] Cyclopentenones,[3] and related saturated cyclopentanones,[4] are key structural subunits often included in medicinal precursors of drug candidates,[5] or as part of polycyclic natural products, such as przewalskin B,[6] norspiculoic acid A or nitidasin[7] (Scheme 1i). In the cyclopentanone series, generation of highly-substituted (hindered) skeletons remains a general challenge requiring, in addition, the stereocontrol of *trans*- or *cis*-fused junctions.[8]

As mentioned earlier, radical-mediated synthesis of polycyclic molecules is a recognized strategy using, most often, intramolecular Giese reactions of carbon-centered radicals onto neighboring olefin(s).[9] Conditions of radical formation and the size of the resulting ring(s) are key parameters that control addition regio- and stereoselectivity.[10] Cyclizations leading to the formation of 5- or 6-membered rings have been particularly studied.[11] Reliable prognostics on such cyclizations are possible thanks to many seminal contributions and Beckwith's radical rules in particular.[12] Also, visible light-induced and photoredox catalyzed reactions have transformed the field of radical-mediated processes leading to a large array of novel synthetic methodologies.[13] In this regard, formations of cyclized products by intramolecular additions after photoreduction of C–X bonds (X = halogen, chalcogen, *etc.*) are key.[13b,14] Most often, *n-exo-trig* regioselectivity is observed primarily, over *n* + 1-*endo-trig* pathways (Scheme 1ii).[15] Of note, Blakey *et al.* reported a switchable regioselective 6-*endo*/5-*exo* photoredox catalyzed cyclization.[16] The selectivity arose from different HAT rates; the 5-*exo* product being obtained with a polarity-matched thiol HAT process, while using Hantszch ester (**HE**) gave the 6-*endo* product.

Previously, using cyclic ketones **1** and α-diazomalonates[17] as reactants (Scheme S1), a direct synthesis of malonate enol ethers **2** was reported under [CpRu(N≡CCH$_3$)$_3$][BAr$_F$] catalysis;[18] the resulting adducts being readily functionalized

[a]*Department of Organic Chemistry, University of Geneva, Quai Ernest Ansermet 30, CH-1211 Geneva 4, Switzerland. E-mail: Jerome.Lacour@unige.ch*
[b]*Laboratory of crystallography, University of Geneva, Quai Ernest Ansermet 24, CH-1211 Geneva 4, Switzerland*
†These authors contributed equally to the work.

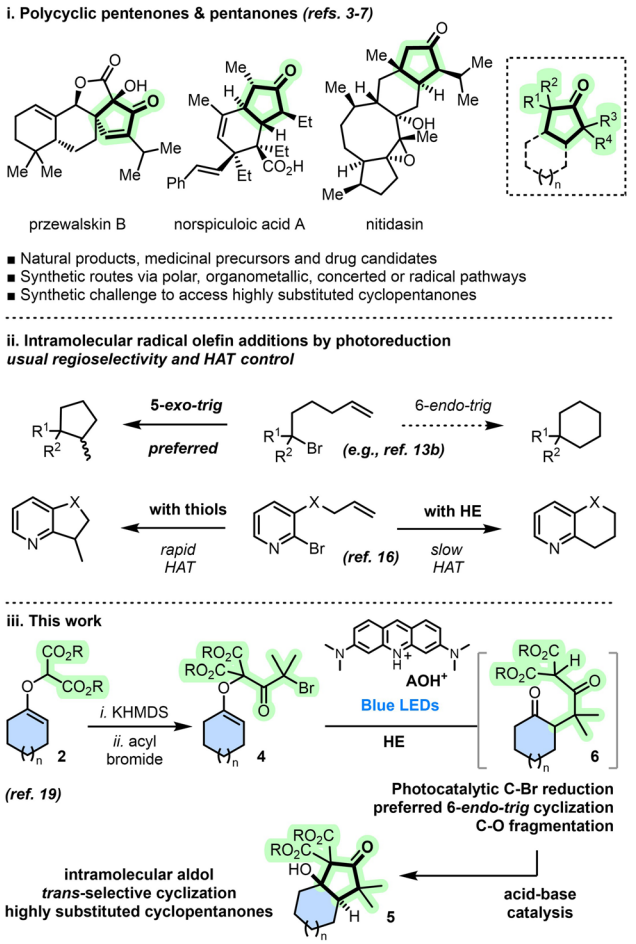

Scheme 1 Polycyclic pentenones and pentanones. Photoreductive radical cyclizations. Synthetic strategy toward highly substituted [*n*.3.0] bicyclic derivatives. **AOH**$^+$ = acridinium orange photocatalyst.

under basic conditions to afford malonate alkylation products.[19] Herein, to harness regioselective radical reactivity and later achieve densely-functionally cyclopentanones, the acylation of enol ethers **2** with 2-bromo-2-methylpropanoyl bromide **3** was pursued to produce substrates of type **4**. Subsequent photoredox conditions afford α-branched ketones that cyclize under mild acidic conditions to form densely-functionalized [*n*.3.0] bicyclic products **5** (*n* = 4, 5, 10) (Scheme 1iii). This novel cyclization sequence, involving two independent C–C bond forming reactions and one original C–O cleavage, generates *trans*-fused bicyclo[4.3.0]nonanes exclusively. Mechanistic studies reveal a dichotomic nature of the photoredox initiation and a possible competition between 5-*exo-trig* and 6-*endo-trig* pathways, generally in favor of the second by virtue of radical philicity matching.[20] An unusual C–O fragmentation and hydrogen atom transfer (HAT) reactions liberate α-branched cyclic ketones of type **6** that are ideally suited for intramolecular aldol/ring closure reactions happening under mild acidic conditions with *trans*-selectivity only.

Table 1 Optimization of the reaction conditions[a]

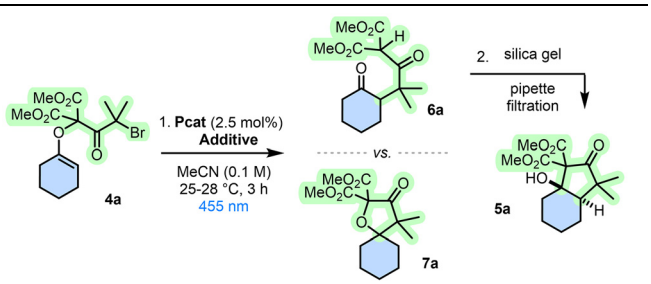

Entry	Photocatalyst (PCat)	Additive	Yield 5a (%)	Ratio (6a/7a)[b]
1	$Ir(ppy)_3$	DIPEA (10 equiv.)	48 (43)[c]	85/15
2	$[Ir(dFCF_3ppy)_2(bpy)]PF_6$	DIPEA (10 equiv.)	50	90/10
3	$[Ir(dFCF_3ppy)_2(bpy)]PF_6$	DIPEA (10 equiv.), **HE** (5 equiv.)	60	82/18
4	$[Ir(dFCF_3ppy)_2(bpy)]PF_6$	**HE** (10 equiv.)	72	91/9
5	$Ir(ppy)_3$	**HE** (2.5 equiv.)	70	92/8
6	Rose bengal	**HE** (2.5 equiv.)	60	96/4
7	Eosin Y	**HE** (2.5 equiv.)	68	91/9
8	**Acridine orange**	**HE (2.5 equiv.)**	**72 (66)**[c]	**92/8**
9	Acridine orange	None	Traces	—
10	Acridine orange	**HE** (2.5 equiv.)	n.r.[d]	—
11	None	**HE** (2.5 equiv.)	19	92/8

[a] Reaction conditions: **4a** (0.05 mmol), **PCat** (2.5 mol%), additive, MeCN (0.1 M), 25–28 °C, blue LEDs, 3 h. Yields determined by ^{1}H-NMR spectroscopy using 1,3,5-trimethoxybenzene as internal standard. DIPEA: *N*,*N*-Diisopropylethylamine. [b] Ratios between **6a** and **7a** were determined by ^{1}H NMR analysis. [c] Isolated yields in parenthesis. [d] Without light. n.r.: no reaction.

Results and discussion

In the context of cyclization strategies, it was then enticing to use compounds **2** and their malonate subunits to introduce halogenated chains under basic conditions (substrates **4**, Table 1 and Scheme 2) and study subsequent reductions under photoredox conditions. Upon generation of electrophilic α-keto radicals, ring formation ought to occur onto the nucleophilic end of the enol ether moiety providing an effective discrimination and a preferred 6-*endo* regioselectivity. Preliminary studies were performed using enol ether **4a** made from **2a** by treatment with KHMDS (2.0 equiv.) at 25 °C. After rapid and quantitative deprotonation of the malonate group, addition of 2-bromo-2-methylpropanoyl bromide **3** (1.5 equiv.) afforded adduct **4a** (64%). Then, under blue LED irradiation (λ_{max} 455 nm) using $Ir(ppy)_3$ (2.5 mol%) as photocatalyst (PCat) and diisopropylethylamine (DIPEA) as reductant and hydrogen donor (10 equiv.), the targeted reactivity was immediately observed in acetonitrile at 25–28 °C (Table 1, entry 1). ^{1}H NMR analyses of crude reaction mixtures were initially ambiguous as large differences were observed between spectra measured before and after a short filtration over a SiO_2 plug.[21] In the latter case, spectra revealed an excellent conversion of **4a** to major product **5a** obtained as a single stereoisomer. This product was isolated upon silica gel chromatography (43%). Yet, NMR investigations of **5a** were not agreeing

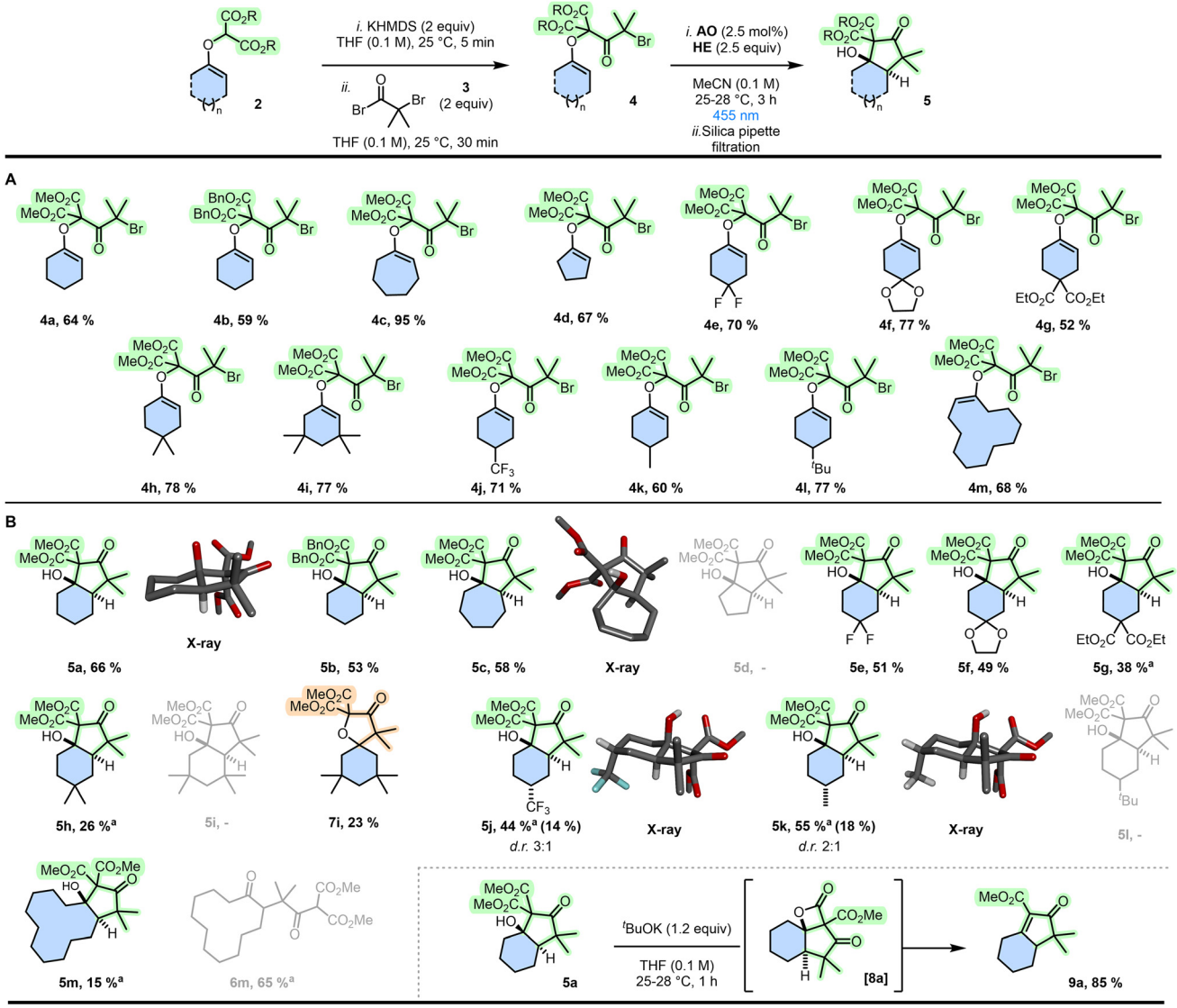

Scheme 2 (A) Acylated malonate enol ethers **4a** to **4m**. (B) Hydroxylated *trans*-bicycles **5a** to **5m**. [a] Yields determined by ^{1}H-NMR spectroscopy using 1,3,5-trimethoxybenzene as internal standard. Isolated yield of the major diastereomer in parenthesis. In grey, lack of product formation or open-armed product obtained.

with structures derived from simple 5-*exo-trig* or 6-*endo-trig* cyclization pathways. The connectivity indicated the occurrence of a rearrangement that could only be untangled upon X-ray analysis (CCDC 2058766). Single crystals of **5a** were obtained by diffusion in a mixture of methylene chloride and pentane. The structural determination revealed a [4.3.0] bicycle with two *trans*-fused carbocycles; a cyclohexane and a densely-functionalized cyclopentanone. Care was then taken to unravel the reactivity prior to the silica gel treatment, *i.e.* before the cyclization to **5a**. All crude NMR data pointed toward α-branched cyclohexanone **6a**, which cannot be isolated. Further analysis of the crude mixture indicated, in retrospect, the presence of a minor component corresponding to spiro bicycle **7a** (4–18%, Table 1). The origin of this moiety will be later discussed during the mechanistic analysis but such an occurrence was expected in view of the usual predominance of 5-*exo-trig* cyclization pathways and also results previously-obtained with malonate enol ethers.[19] Given the unusual skeletal rearrangement of **4a** to **6a** and then ***trans*-5a**, the reactivity was investigated further. First, a screen of experimental conditions (Table S1) was performed to improve conversions and yields, an excerpt is detailed in Table 1. Substitution with [Ir(dFCF$_3$ppy)$_2$(bpy)]PF$_6$ as photocatalyst increased the yield up to 50% (entry 2). Additional amounts of **HE** (5 equiv.) were beneficial (**5a**, 60%, entry 3). In effect, **HE** (10 equiv.) could substitute DIPEA entirely (**5a**, 72%, entry 4). Classical Ir(ppy)$_3$ could be used with only 2.5 equivalents of **HE** to form **5a** in 70% (entry 5). Various organic dyes absorbing in blue-green domains were also tested as photocatalysts (entries 6–8, and Table S1), including rose Bengal or eosin Y giving yields of

60% and 68%, respectively (entries 6 and 7). With mildly-reducing acridine orange (**AO**), to a bit of our surprise, bicycle **5a** was still obtained in an effective yield (72%, entry 8); a rationale will be provided later (*vide infra*). Further variations of different Hantzsch esters, solvents, catalyst loading and substrate concentration, did not lead to any additional improvements (Table S1). As expected, reactions do not proceed in the absence of **HE** or blue light (entries 9 and 10). Without **AO**, **5a** is nevertheless obtained in a surprising 19% yield, suggesting that **HE** can also play a photoreducing role (entry 11); this reactivity will be later exploited. Nonetheless, entry 8 combining (i) visible light photoredox catalysis and (ii) a silica gel filtration represented the most effective conditions to **5a**, which were selected for the remainder of the study.

In effect, a series of α-bromo *gem*-dimethyl ketones **4a** to **4m** were prepared from the corresponding malonate enol ethers (Scheme 2A). Overall, the acylation was effective (52–95% yields) under irreversible deprotonation conditions (KHMDS). Then, using conditions from Table 1 (entry 8), *trans*-fused bicyclic compounds **5** were obtained in low to good yields (15–66%, Scheme 2B).[22] First, with **4a**, the reaction was conducted in 1 mmol scale and proceeded without loss of conversion to afford **5a** with a comparable isolated yield (66%). However, performed on a gram scale of starting bromide, the isolated yield of **5a** decreased to 50%. Benzyl malonate enol ether **4b** reacted similarly to give **5b** in slightly lower 53% yield, a possible consequence of the increased steric hindrance. 7-Membered ring **5c** formed efficiently (58%). The *trans* ring fusion was ascertained by X-ray diffraction analysis again (CCDC 2481640, Scheme 2). In the case of cyclopentanone-derived **5d**, which was unproductive, the elevated strain associated with a *trans*-fused [3.3.0] structure[23] is probably responsible for the lack of ring closure observed.[24] 4,4′-Difluorinated enol ether **4e** and dioxolane **4f** reacted to yield **5e** and **5f** in 51% and 49% yields, respectively. However, *gem*-disubstituted **4g** and **4h** afforded the corresponding dimethylated and dicarboxyethylated products **5g** and **5h** in lower 38 and 26% (NMR yields), respectively. Overall, despite a lower productivity for diester **5g**, the presence of (inductive) electron-withdrawing groups at 4,4′-positions seems more favorable. However, strong steric effects preclude cyclization as hexamethylated **5i** could not be formed. Instead of *trans*-fused rings, 5-*exo*-*trig* cyclization is preferred forming the spirocycle adduct **7i** (30% NMR and 23% isolated yields). The diastereoselectivity of the cyclization was briefly studied with 4-trifluoromethyl and 4-methyl-substituted enol ethers **5j** and **5k**. *trans*-Bicycles **5j** (44% NMR yield) and **5k** (55% NMR yield) were obtained as mixtures, with respective 3 : 1 and 2 : 1 diastereomeric ratios (dr). Only the major isomers could be isolated upon chromatography (14% and 18%, respectively); their structures (CCDC 2481641 and 2481639) presenting the 4-CH_3 or 4-CF_3 groups in axial positions. A rationale for the observed stereochemistry is provided in the SI (Scheme S4).[25] However, when the substrate is again strongly hindered or biased sterically like **5l** with the *tert*-butyl substituent, a lack of desired reactivity is obtained. Finally, of importance for the mechanism, [10.3.0] bicycle **5m** was obtained from 12-membered **4m** in a low ^{1}H-NMR yield (15%) but alongside **6m** (63%) as major product. This derivative **6m** is not prone to enolization and cyclization. Yet, this observation of **6m** led us to check how general was the formation of open-arm molecules. In the six-membered ring series, crude mixtures from reactions of **4a** and **4f** were verified immediately after irradiation, only to confirm the presence of α-functionalized cyclohexanones in all instances. The photoredox cyclization therefore stops at the C–O bond fragmentation and the formation of adducts of type **6**. With these mixtures in hand, a small amount of silica gel (pipette filtration) was sufficient to provoke the intramolecular aldol to **5a** and **5f**.[26] Nevertheless, condensations were more reliable under soft-enolization Lewis acid–base conditions.[27] In fact, full conversion was obtained with either $MgCl_2/Et_3N$[28] or LiCl/DBU[27a] to yield **5a** (66%) in 15 and 30 minutes from **6a**, respectively. Finally, care was taken to evaluate the reactivity of the *trans*-fused products of type **5** only to find that the tertiary alcohol group is unreactive under dehydration (*e.g.*, Burgess reagent[29]) or alkylative conditions (*e.g.*, benzyl 2,2,2-trichloroacetimidate[30]). However, upon addition of ^{t}BuOK at 25 °C, hydroxydecarboxylative elimination occurs. Mechanistically, it is proposed that β-lactone [**8a**] is formed and leads to **9a** (85%) upon strain release and CO_2 cleavage.

In parallel, insight into the photocatalytic mechanism (**4a** 1.0 equiv., **AO** 2.5 mol% and HE 2.5 equiv.) was looked for (Fig. 1). Optical and electrochemical data of the reactants provided possible energy pathways upon light excitation (see SI).[31] Absorption and emission spectra of **AO** (Fig. S1) afforded an optical energy gap (E_{00}) of 2.62 eV, with a reported reduction potential in acetonitrile of −2.0 V *vs.* SCE.[32] As a consequence, the excited state **AO*** has E^{red} = +0.62 V (*vs.* SCE) and cannot perform the necessary oxidation of **HE** (E^{ox} = +0.93 V *vs.* SCE) by single electron transfer (SET). The overall process is unproductive ($\Delta G_0 > 0$, see SI).[33] After this observation, the UV-Vis absorption spectrum of the crude reaction was analyzed further and it revealed a lower energy signal upon reaction of **AO** with **HE** in excess, which was matched with protonated acridinium **AOH$^+$** (see Fig. 1IIa). This cationic species possesses all the necessary properties in its excited state to perform photocatalysis (E_{00} = 2.44 eV, E^{red} (**AOH$^+$*/AOH$^\bullet$**) = +1.72 V and E^{ox} (**AOH$^{+\bullet}$/AOH$^+$***) = −1.24 V *vs.* SCE) (Tables S2 and S3). In effect, by irradiating at 455 nm, **AOH$^+$** is efficiently excited and two quenching pathways are then energetically possible, either (*i*) a SET involving the oxidation of **HE** or (*ii*) the direct reduction of enol ether **4a** (E^{red} = −1.0 V *vs.* SCE). In support, with Stern–Volmer experiments, quenching of **AOH$^+$** luminescence (λ_{em} = 525 nm, Φ = 37% and τ = 2.5 ns in acetonitrile) is detected for both **HE** and enol ether **4a** with kinetic quenching constants (k_q) of 1.1 × 10^{10} M^{-1} s^{-1} and 1.6 × 10^9 M^{-1} s^{-1}, respectively (Fig. 1IIb). While quenching of **HE** is 10-fold faster than that of the enol ether **4a**, quenching efficiencies (η) are similar with values of 28% and 20%, taking into account the available concentrations of **HE** and **4a** in solution during the photocatalytic reaction (Fig. S10–S13).[34] Overall, path *i* (Fig. 1) remains more favorable than path *ii*

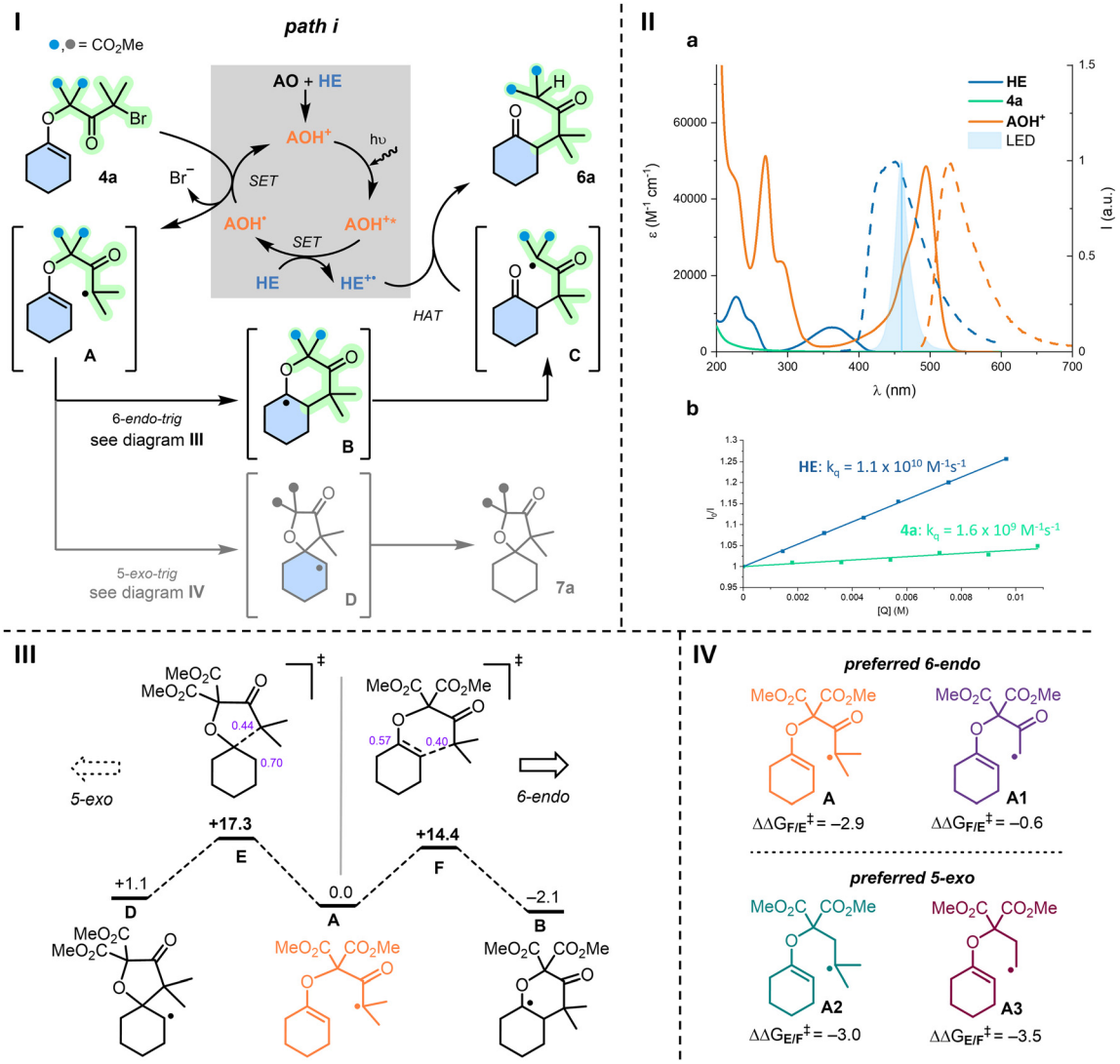

Fig. 1 (I) Synthesis of open-chained ketone **6a** and spiro derivative **7a** *via* 6-*endo*-*trig* (major, black) and 5-*exo*-*trig* (minor, grey) closures under photocatalysis (path *i*, **AOH**$^+$, λ_{exc} 455 nm). (II) (a) Absorption and normalized emission spectra of reaction components in air-equilibrated acetonitrile 20–23 °C with concentrations 1 × 10^{-5} to 5 × 10^{-6} M and (b) Stern–Volmer plot of the luminescence quenching of **AOH**$^+$ upon increasing concentration of quencher. Quenching experiments were conducted in dry acetonitrile under N_2 atmosphere with **AOH**$^+$ (1 × 10^{-5} M), the emission intensity was followed at λ = 529 nm; I_0 is the intensity before and I after adding the quencher, [**Q**] stands for concentration of the quencher, in which **Q** is either **HE** (path *i*, this figure) or **4a** (path *ii*, Scheme S2). (III) Gibbs free energy analysis of 5-*exo* *vs.* 6-*endo* cyclizations from first radical **A** to bicyclic **B** or spiro **D** radicals, and respective transition states **F** and **E**. (IV) Comparison of **A** with theoretical **A1**, **A2** and **A3** radicals, and subsequent regioselectivity ($\Delta\Delta G^{\ddagger}$, kcal mol^{-1}).

(Scheme S2) and the difference in efficiencies increases over time as **4a** is progressively consumed (Fig. S12). In any case, satisfactorily, both paths *i* and *ii* lead to the same product. With path *i*, shown in Fig. 1I, after formation of **AOH**$^{\bullet}$ by quenching of **AOH**$^{+}$* with **HE**, reduction of substrate **4a** by SET leads to α-keto radical **A**.[44] With path *ii*, displayed in Scheme S2, intermediate **A** is formed directly by reaction of **4a** with **AOH**$^{+}$*. Then, independent of its origin, **A** undergoes a preferred 6-*endo*-*trig* cyclization to form **B**. Subsequent C–O cleavage occurs and affords stabilized tertiary malonyl **C**. Such homolytic C–O cleavage seems to be original to this transformation. Then, the highly electrophilic radical cannot readily cyclize to the intramolecular δ-ketone; preferred HAT of **C** with either **HE** or protonated **HE**$^{+}$ (ref. 35) must occur and yield open-chain products **6** observed in crude mixtures, for **5m** in particular. In terms of regioselectivity, confirmation was brought by computational analysis of the preferred 6-*endo*-*trig* (**A** → **B**) over the 5-*exo*-*trig* (**A** → **D**) cyclization pathways, both kinetically ($\Delta G^{\ddagger}$ = −2.9 kcal mol^{-1}) and thermodynamically (ΔG° = −3.2 kcal mol^{-1}) (Fig. 1III).

As the regioselectivity depended most probably on a philicity matching of first radical **A** with the enol ether moiety, care was taken to evaluate theoretically the influence of the substituents adjacent to the radical carbon center of **A**. DFT calcu-

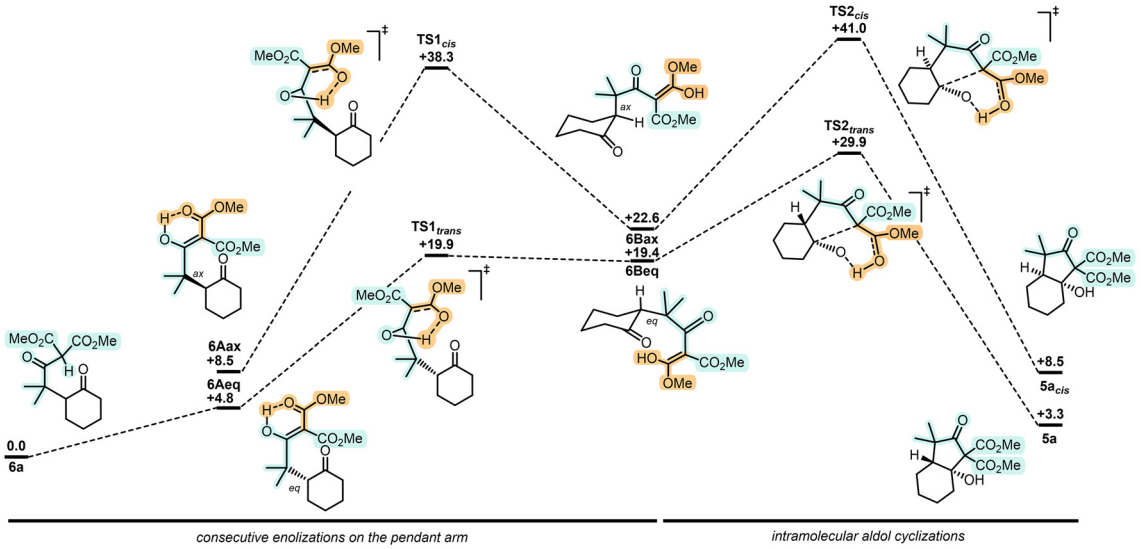

Scheme 3 Computed reaction paths from synthetic intermediate **6a** to *trans*-fused **5a** and putative **5a**$_{cis}$. Gibbs free energies in kcal mol^{-1}.

lations using hypothetical intermediates **A1** (*gem*-Me omitted), **A2** (α-carbonyl omitted) and **A3** (both elements missing) were executed and results compared to that of original **A** (Fig. 1IV). Energy barriers were calculated for 6-*endo* (**As** → **Bs**) or 5-*exo* (**As** → **Ds**) pathways *via* transition states **Fs** and **Es**, respectively (Fig. S15). As expected, in view of the polarization of the electron-rich alkene and its more nucleophilic terminal end, electrophilic α-carbonyl radicals **A** and **A1** favor the formation of **B** and **B1** *via* transition states **F** and **F1** ($\Delta\Delta G^{\ddagger}_{F/E}$ = −2.9 and −0.6 kcal mol^{-1}), respectively.[36] Then, changing the nature of radicals from electrophilic to nucleophilic, **A2** and **A3** formed preferentially spiro 5-membered rings through transitions states **E2** and **E3** ($\Delta\Delta G^{\ddagger}_{E/F}$ = −3.0 and −3.5 kcal mol^{-1}), respectively. Then, with a clear explanation for the formation of open-chained derivatives **6**, ring closures to bicyclic *trans*-fused **5** were also investigated computationally using mild Brønsted acid conditions as model (Scheme 3).[37] Direct cyclization of ketone **6a**, used as reactant, through a concerted transition state with proton-transfer and C–C bond formation occurring at the same time was unsuccessful.[38] Then, we proceeded *via* all possible enols derived from **6a**. Intermediates **6Aax** and **6Aeq** model most-stable enols with either axial or equatorial orientation of the pendant arm, and intermediates **6Bax** and **6Beq**, necessary for the reactivity, are the enols formed on the side of the malonate chains. The lower reaction pathway requires the formation of enol **6Beq** prior to the intramolecular aldol. Its geometry favors a pre-organization of the arm leading to a late 6-membered transition state (TS2-*trans*) that achieves the *trans*-fused bicycle **5a** by the lower activation barrier computed so far ($\Delta G^{\ddagger}$ = +29.9 kcal mol^{-1}).[39] In fact, without the presence of enol **6Beq**, the cyclization from **6Aeq** was located at +50.6 kcal mol^{-1} as it models a less favored 7-membered ring transition state (Scheme S3). For good measure, analogous transition state TS2-*cis*, which would be necessary to reach a *cis*-fused bicycle, was located at 41.0 kcal mol^{-1}, more than 10 kcal mol^{-1} higher than TS2-*trans*, in agreement with experimental observation. Additionally, formation of precursor **6Bax** is strongly unfavored due to the

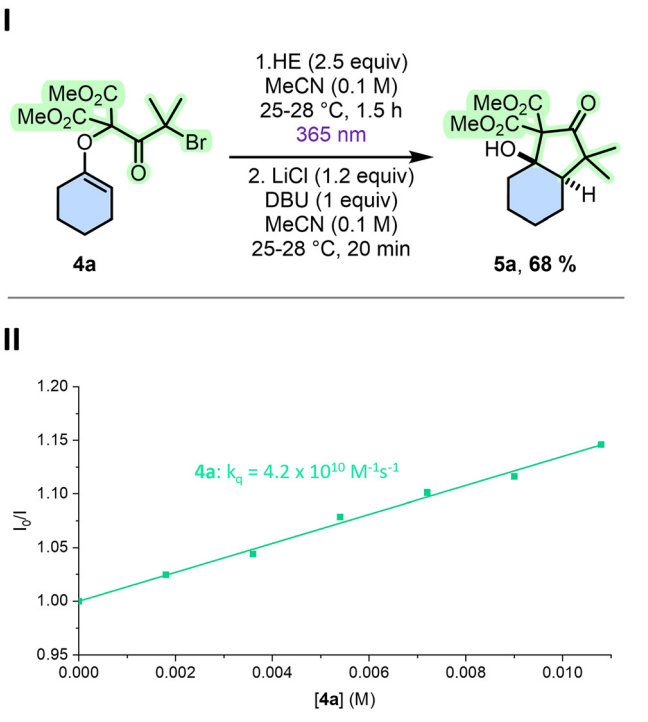

Fig. 2 (I) Cyclization with **HE** under UV light (365 nm) followed by soft enolization/cyclization. Yield determined by ^{1}H-NMR spectroscopy using 1,3,5-trimethoxybenzene as internal standard. (II) Stern–Volmer plot of the luminescence quenching of **HE** upon increasing concentration of **4a**. Quenching experiments were conducted in dry acetonitrile under N_2 atmosphere with **HE** (5 × 10^{-5} M), the emission intensity was followed at λ = 455 nm; I_0 is the intensity before and I after adding the quencher **4a**.

required enol geometrical isomerization upon proton transfer from **6Aax**. This motion breaks the π-delocalization and the H···O interaction, *via* TS1-*cis* ($\Delta G^{\ddagger}$ = +38.3 kcal mol^{-1}) which is also far too high. Preferred formation of *trans*-fused bicycle **5a** is hence justified computationally.

Finally, literature analysis indicated that **HE** can directly promote photoreductive processes, including selective debromination of α-bromo ketones.[40] In this context, reactions were tested without photocatalyst under strict anaerobic conditions but employing a LED of higher energy. Satisfactorily, productive results were obtained while irradiating at 365 nm as product **5a** was isolated in 68% yield (Fig. 2I).[41] In fact, with enol ether **4a** as substrate, **HE** (E_{00} = 3.06 eV and E^{ox} = +0.93 V *vs.* SCE) acts as photoreductant (**HE*** having E^{*ox} = −2.13 V). As it could be expected, Stern–Volmer analysis with gradual additions of **4a** revealed an emission quenching of **HE** (Φ = 1.7% and τ = 0.32 ns in DMSO, of comparable polarity to acetonitrile). The SET process is characterized by a quenching constant of k_q = 4.2 × 10^{10} M^{-1} s^{-1} (Fig. 2II), corresponding to an efficiency η of 57% indicating a faster and more effective activation than the reactions derived from **AOH**$^+$ as photocatalyst. In the present case, full reduction of **4a** is enacted with 2.5 equivalents of **HE** in 1.5 hours only. Further investigation demonstrated a lack of photodecarbonylation after prolonged UV irradiation.[42]

Conclusions

Highly functionalized *trans*-fused [*n*.3.0] bicycles (**5**) were synthesized (*n* = 4, 5, 10). The synthetic method combines photoinduced 6-*endo-trig* Giese additions with mild intramolecular aldol cyclizations. In practice, two distinct photoredox methods were considered. On one hand, photocatalytic conditions were developed using acridinium orange as a mild photocatalyst in the blue range (λ_{exc} = 455 nm), in combination with Hantzsch ester **HE**, which serves as both the reducing agent and hydrogen donor. On the other hand, **HE** was used for its own photoreductive properties at higher energy (λ_{exc} = 365 nm). Overall, these cyclization methods allow for the formation of unusually-dense *trans*-fused hydrindanones derivatives. While the process was mostly demonstrated for enol ethers made from cyclohexanone backbone, extension to other ring size remains a possibility. Finally, DFT calculations validate all the mechanistic pathways and regioselectivity in favor of a philicity matching of the electrophilic radical and the polar electron-rich nature of the malonate enol ether.

Conflicts of interest

There are no conflicts to declare.

Data availability

The data that support the findings of this study are openly available in yareta.unige.ch at **https://doi.org/10.26037/yareta:ehkvr2be4za3bchnlyjv6pgeie**. It will be preserved for 10 years.

Supplementary information (SI) is available. See DOI: **https://doi.org/10.1039/d5qo01635e**.

CCDC 2058766 and 2481639–2481641 contain the supplementary crystallographic data for this paper. These data can be obtained free of charge from The Cambridge Crystallographic Data Centre *via* **www.ccdc.cam.ac.uk**/structures.[43a–d]

Acknowledgements

We thank the University of Geneva and the Swiss National Science Foundation for financial support (Grant 200020-207539 to J.L.). We thank Prof. Philippe Renaud (Bern) and Dr Fabrice Dénès (Nantes) for helpful discussions. The computations were performed at University of Geneva (organic chemistry department). Open access funding was provided by the University de Geneva.

References

1 (*a*) P. S. Baran, *J. Am. Chem. Soc.*, 2018, **140**, 4751–4755; (*b*) K. C. Nicolaou and T. Montagnon, *Molecules that changed the world: a brief history of the art and science of synthesis and its impact on society*, Wiley-VCH, Weinheim, 2008; (*c*) W. Liu, B. Hong, J. Wang and X. Lei, *Acc. Chem. Res.*, 2020, **53**, 2569–2586; (*d*) D. J. Newman and G. M. Cragg, *J. Nat. Prod.*, 2020, **83**, 770–803.

2 (*a*) N. Müller, T. Magauer and O. Kováč, *J. Org. Chem.*, 2025, **90**, 5083–5092; (*b*) S. J. Kwon and D. Y. Kim, *Chem. Rec.*, 2016, **16**, 1191–1203; (*c*) I. Omae, *Coord. Chem. Rev.*, 2011, **255**, 139–160; (*d*) J. Liao, X. Yang, L. Ouyang, Y. Lai, J. Huang and R. Luo, *Org. Chem. Front.*, 2021, **8**, 1345–1363; (*e*) S. H. Kyne, M. Clémancey, G. Blondin, E. Derat, L. Fensterbank, A. Jutand, G. Lefèvre and C. Ollivier, *Organometallics*, 2018, **37**, 761–771.

3 J. Jose and T. V. Mathew, *Tetrahedron*, 2024, **150**, 133747.

4 D. T. Hog, P. Mayer and D. Trauner, *J. Org. Chem.*, 2012, **77**, 5838–5843.

5 (*a*) C. Djerassi, L. Miramontes, G. Rosenkranz and F. Sondheimer, *J. Am. Chem. Soc.*, 1954, **76**, 4092–4094; (*b*) H. Li, H. J. Lee, Y. H. Ahn, H. J. Kwon, C.-Y. Jang, W.-Y. Kim and J.-H. Ryu, *Biochem. Biophys. Res. Commun.*, 2014, **443**, 132–137.

6 G. Xu, A.-J. Hou, Y.-T. Zheng, Y. Zhao, X.-L. Li, L.-Y. Peng and Q.-S. Zhao, *Org. Lett.*, 2007, **9**, 291–293.

7 (*a*) F. Berrue, O. P. Thomas, R. Laville, S. Prado, J. Golebiowski, R. Fernandez and P. Amade, *Tetrahedron*, 2007, **63**, 2328–2334; (*b*) N. Kawahara, M. Nozawa, D. Flores, P. Bonilla, S. Sekita, M. Satake and K.-I. Kawai, *Chem. Pharm. Bull.*, 1997, **45**, 1717–1719; (*c*) N. A. Eddy and P. Ichalkaranje, in *Molecules*, 2016, vol. 21; (*d*) M. J. Brienne, A. Heymes, J. Jacques, G. Snatzke, W. Klyne and S. R. Wallis, *J. Chem. Soc. C*, 1970, 423–432.

8 P. Jankowski, S. Marczak and J. Wicha, *Tetrahedron*, 1998, **54**, 12071–12150.

9 (*a*) B. Giese, *Angew. Chem., Int. Ed. Engl.*, 1983, **22**, 753–764; (*b*) P. Renaud, *Chimia*, 2001, **55**, 1045.
10 T. RajanBabu, *Acc. Chem. Res.*, 1991, **24**, 139–145.
11 (*a*) K. J. Romero, M. S. Galliher, D. A. Pratt and C. R. J. Stephenson, *Chem. Soc. Rev.*, 2018, **47**, 7851–7866; (*b*) H. Y. Song, J. M. Joo, J. W. Kang, D.-S. Kim, C.-K. Jung, H. S. Kwak, J. H. Park, E. Lee, C. Y. Hong, S. Jeong, K. Jeon and J. H. Park, *J. Org. Chem.*, 2003, **68**, 8080–8087; (*c*) H. Zhang, S. Ma, Z. Xing, L. Liu, B. Fang, X. Xie and X. She, *Org. Chem. Front.*, 2017, **4**, 2211–2215; (*d*) D. P. Curran and C. T. Chang, *J. Org. Chem.*, 1989, **54**, 3140–3157; (*e*) S. Pradhan and S. Das, *Helv. Chim. Acta*, 2025, **108**, e202400206; (*f*) J. Xuan and A. Studer, *Chem. Soc. Rev.*, 2017, **46**, 4329–4346.
12 (*a*) A. L. J. Beckwith and C. H. Schiesser, *Tetrahedron*, 1985, **41**, 3925–3941; (*b*) I. V. Alabugin and K. Gilmore, *Chem. Commun.*, 2013, **49**, 11246–11250.
13 (*a*) T. P. Yoon, M. A. Ischay and J. Du, *Nat. Chem.*, 2010, **2**, 527–532; (*b*) J. W. Tucker, J. D. Nguyen, J. M. R. Narayanam, S. W. Krabbe and C. R. J. Stephenson, *Chem. Commun.*, 2010, **46**, 4985–4987; (*c*) N. A. Romero and D. A. Nicewicz, *Chem. Rev.*, 2016, **116**, 10075–10166; (*d*) M. H. Shaw, J. Twilton and D. W. C. MacMillan, *J. Org. Chem.*, 2016, **81**, 6898–6926; (*e*) J. J. Douglas, M. J. Sevrin and C. R. J. Stephenson, *Org. Process Res. Dev.*, 2016, **20**, 1134–1147; (*f*) A. L. Gant Kanegusuku and J. L. Roizen, *Angew. Chem., Int. Ed.*, 2021, **60**, 21116–21149; (*g*) S. P. Pitre and L. E. Overman, *Chem. Rev.*, 2022, **122**, 1717–1751; (*h*) J. D. Bell and J. A. Murphy, *Chem. Soc. Rev.*, 2021, **50**, 9540–9685; (*i*) M. A. Ashley, C. Yamauchi, J. C. K. Chu, S. Otsuka, H. Yorimitsu and T. Rovis, *Angew. Chem., Int. Ed.*, 2019, **58**, 4002–4006.
14 (*a*) C.-J. Wallentin, J. D. Nguyen, P. Finkbeiner and C. R. J. Stephenson, *J. Am. Chem. Soc.*, 2012, **134**, 8875–8884; (*b*) R. K. Dhungana, A. Granados, V. Ciccone, R. T. Martin, J. Majhi, M. Sharique, O. Gutierrez and G. A. Molander, *ACS Catal.*, 2022, **12**, 15750–15757.
15 (*a*) C. Walling and A. Cioffari, *J. Am. Chem. Soc.*, 1972, **94**, 6059–6064; (*b*) Y. Yamashita, Y. Ogasawara, T. Banik and S. Kobayashi, *J. Am. Chem. Soc.*, 2023, **145**, 23160–23166.
16 M. C. Maust, C. M. Hendy, N. T. Jui and S. B. Blakey, *J. Am. Chem. Soc.*, 2022, **144**, 3776–3781.
17 S. P. Green, K. M. Wheelhouse, A. D. Payne, J. P. Hallett, P. W. Miller and J. A. Bull, *Org. Process Res. Dev.*, 2020, **24**, 67–84.
18 (*a*) T. Achard, L. Egger, C. Tortoreto, L. Guénée and J. Lacour, *Helv. Chim. Acta*, 2020, **103**, e2000190; (*b*) E. P. Kündig and F. R. Monnier, *Adv. Synth. Catal.*, 2004, **346**, 901–904.
19 J. Viñas-Lóbez, G. Levitre, A. de Aguirre, C. Besnard, A. I. Poblador-Bahamonde and J. Lacour, *ACS Org. Inorg. Au*, 2021, **1**, 11–17.
20 F. Parsaee, M. C. Senarathna, P. B. Kannangara, S. N. Alexander, P. D. E. Arche and E. R. Welin, *Nat. Rev. Chem.*, 2021, **5**, 486–499.
21 This observation will be later considered and explained. It will lead to the development of soft enolization conditions to promote the final cyclization from **6** to closed *trans*-fused **5**.
22 As noted in ref. 15*b*, formation of bicyclic adducts upon reductive olefin radical addition seems to give lower yields than acyclic or monocyclic derivatives.
23 Of note, as it could be expected, previous calculations indicate a thermodynamic preference for the *cis*- over the *trans*-isomer in bicyclo[3.3.0]octanones adducts. SeeH. L. Gordon, S. Freeman and T. Hudlický, *Synlett*, 2005, 2911–2914.
24 Three main derivatives compose the crude reaction mixture including (i) the open-chain ketone derivative of type **6** made by 6-*endo-trig* cyclization and malonate cleavage and (ii) the spiro derivative made by 5-*exo-trig* cyclization. The third derivative was not identified. Concerning the open-chain ketone, soft enolization conditions (*vide infra*) could not afford the cyclized product.
25 The selectivity originates in the (moderately) selective first addition of the tertiary radical onto the α-face of the alkene when the 4-substituent (CF_3 or Me) occupies an equatorial position.
26 Activated silica was shown to promote intramolecular cyclization on α,β-unsaturated 1,2-diones. See; E. A. Uhrich, W. A. Batson and M. A. Tius, *Synthesis*, 2006, 2139–2142.
27 (*a*) M. A. Blanchette, W. Choy, J. T. Davis, A. P. Essenfeld, S. Masamune, W. R. Roush and T. Sakai, *Tetrahedron Lett.*, 1984, **25**, 2183–2186; (*b*) D. F. Netz and J. L. Seidel, *Tetrahedron Lett.*, 1992, **33**, 1957–1958; (*c*) D. A. Evans, M. J. Dart, J. L. Duffy and D. L. Rieger, *J. Am. Chem. Soc.*, 1995, **117**, 9073–9074.
28 M. W. Rathke and P. J. Cowan, *J. Org. Chem.*, 1985, **50**, 2622–2624.
29 A. Chandra, S. R. Cheekatla, V. K. Vishwakarma and D. Kumar, *Asian J. Org. Chem.*, 2025, **14**, e202500338.
30 P. Eckenberg, U. Groth, T. Huhn, N. Richter and C. Schmeck, *Tetrahedron*, 1993, **49**, 1619–1624.
31 (*a*) V. Balzani, P. Ceroni and A. Juris, *Photochemistry and photophysics: concepts, research, applications*, Wiley-VCH, Weinheim, 2014; (*b*) N. G. Connelly and W. E. Geiger, *Chem. Rev.*, 1996, **96**, 877–910.
32 T. T. Eisenhart and J. L. Dempsey, *J. Am. Chem. Soc.*, 2014, **136**, 12221–12224.
33 Formation of an electron donor acceptor (EDA) complex was furthermore ruled out by recording absorption spectra of **AO** while increasing the concentration of enol ether **4a**.
34 As the quantity of **HE** is saturated in the reaction mixture ($[\mathbf{HE}]_{sat}$ = 0.02 M, SI), its concentration can be considered constant in time. Also, substrate **4a** is quickly consumed lowering further its quenching efficiency (see SI, section S8).
35 S. Azizi, G. Ulrich, M. Guglielmino, S. le Calvé, J. P. Hagon, A. Harriman and R. Ziessel, *J. Phys. Chem. A*, 2015, **119**, 39–49.
36 This theoretical analysis also explains the minimal amounts of spiro adduct **7a** (*ca.* 7% NMR yield) in view of

the relatively small difference in energy between transition states **E** and **F**.

37 (*a*) T. Kobayashi, H. Abe and H. Ito, *J. Synth. Org. Chem., Jpn.*, 2019, **77**, 1086–1095; (*b*) N. R. Cichowicz, W. Kaplan, Y. Khomutnyk, B. Bhattarai, Z. Sun and P. Nagorny, *J. Am. Chem. Soc.*, 2015, **137**, 14341–14348.

38 Several relaxed scans searching for this transition state to achieve the formation of the *trans*-fused bicycles **5a** observed experimentally, where always going up in energy. The relative energy performing this transition state was over 70 kcal mol^{-1}, which was not in agreement with experimental observations and, therefore, this reaction path was discarded.

39 Currently, the activation barrier of 29.9 kcal mol^{-1} is high in relation with the experimental room temperature conditions. Computationally, only one explicit proton is considered in the calculations, while experiments require general acidic conditions. This probably indicates that more than one proton is involved in the proton transfer or in the stabilisation of the TS *via* H-bonding. As a consequence, a lower energy barrier would result at room temperature.

40 (*a*) S. Fukuzumi, K. Hironaka and T. Tanaka, *J. Am. Chem. Soc.*, 1983, **105**, 4722–4727; (*b*) G. Li, R. Chen, L. Wu, Q. Fu, X. Zhang and Z. Tang, *Angew. Chem., Int. Ed.*, 2013, **52**, 8432–8436; (*c*) K. Nakajima, S. Nojima, K. Sakata and Y. Nishibayashi, *ChemCatChem*, 2016, **8**, 1028–1032; (*d*) L. Buzzetti, A. Prieto, S. R. Roy and P. Melchiorre, *Angew. Chem.*, 2017, **129**, 15039–15043; (*e*) D.-L. Zhu, Q. Wu, H.-Y. Li, H.-X. Li and J.-P. Lang, *Chem. – Eur. J.*, 2020, **26**, 3484–3488; (*f*) G. Suresh Yedase, S. Venugopal, A. P. and V. Reddy Yatham, *Asian J. Org. Chem.*, 2022, **11**, e202200478; (*g*) S. Patel, A. Chakraborty and I. Chatterjee, *Org. Lett.*, 2023, **25**, 8246–8251; (*h*) N. Li, J.-L. Si and M.-Y. Xu, *Chem. – Eur. J.*, 2025, **31**, e202404116.

41 The reaction was performed in a one-pot procedure using an additional 2.5 equivalents of DBU in the initial reaction mixture. Under such conditions, the yield of **5a** dropped to 15%. In addition, degradation of starting material **4a** was observed by ^{1}H NMR spectroscopy along with other unidentified by-products.

42 J. E. Starr and R. H. Eastman, *J. Org. Chem.*, 1966, **31**, 1393–1402.

43 (*a*) CCDC 2058766: Experimental Crystal Structure Determination, 2026, DOI: **10.5517/ccdc.csd.cc2739th**; (*b*) CCDC 2481639: Experimental Crystal Structure Determination, 2026, DOI: **10.5517/ccdc.csd.cc2p9bw7**; (*c*) CCDC 2481640: Experimental Crystal Structure Determination, 2026, DOI: **10.5517/ccdc.csd.cc2p9bx8**; (*d*) CCDC 2481641: Experimental Crystal Structure Determination, 2026, DOI: **10.5517/ccdc.csd.cc2p9by9**.

44 In path *i*, the second single-electron transfer leading to **A** from **4a** is not thermodynamically allowed *stricto-senso* but it could be promoted by an *in-situ* equilibrium between $\mathbf{AOH}^{\bullet}$ and $\mathbf{AO}^{\bullet}$. Alternatively, excitation of $\mathbf{AOH}^{\bullet}$ could occur. Both $\mathbf{AO}^{\bullet}$ and $\mathbf{AOH}^{\bullet *}$ are strongly reductive species.